

Core momentum distribution in two-neutron halo nuclei

L. A. Souza ^a, F. F. Bellotti ^{a,b}, M. T. Yamashita ^c,
T. Frederico ^a ¹ and Lauro Tomio ^{c,d}

^a*Instituto Tecnológico de Aeronáutica, DCTA, 12228-900, S. José dos Campos, Brazil.*

^b*Department of Physics and Astronomy, Aarhus University, DK-8000 Aarhus C, Denmark.*

^c*Instituto de Física Teórica, UNESP - Universidade Estadual Paulista, 01156-970, São Paulo, Brazil*

^d*Centro de Ciências Naturais e Humanas, Universidade Federal do ABC, 09210-580, Santo André, Brazil.*

Abstract

The core momentum distribution of a weakly-bound neutron-neutron-core exotic nucleus is computed within a renormalized zero-range three-body model, with interactions in the s-wave channel. The halo wave-function in momentum space is obtained by using as inputs the two-body scattering lengths and the two-neutron separation energy. The core momentum densities are computed for ^{11}Li , ^{14}Be , ^{20}C and ^{22}C . The model describes the experimental data for ^{11}Li , ^{14}Be and to some extent ^{20}C . The recoil momentum distribution of the ^{20}C from the breakup of ^{22}C nucleus is computed for different two-neutron separation energies, and from the comparison with recent experimental data the two-neutron separation energy is estimated in the range $100 \lesssim S_{2n} \lesssim 400$ KeV. The recoil momentum distribution depends weakly on the neutron- ^{20}C scattering length, while the matter radius is strongly sensitive to it. The expected universality of the momentum distribution width is verified by also considering excited states for the system.

Key words: Binding energies, Faddeev equation, halo-nuclei, three-body system

1 Introduction

The core recoil momentum distribution of radioactive two-neutron halo nuclei close to the drip line, extracted from breakup reactions at few hundreds

¹ Corresponding author: tobias@ita.br

MeV/A, are expected to be quite useful in order to get insights on the underlying neutron-neutron-core structure of these exotic nuclei [1,2]. This is particularly clear in the example of ^{11}Li breakup in a carbon target at 800 MeV/A [1], where the momentum distribution is characterized by the sum of two distributions, a narrow one with $\sigma = 21(3)\text{MeV}/c$ and a wide one with $\sigma = 80\text{ MeV}/c$, given that σ^2 is the variance associated with a normal distribution. The narrow momentum distribution should be associated with a large configuration of the two neutrons forming a halo structure. In this case the breakup occurs when the two neutrons are found quite far from the core, corresponding to a weakly-bound three-body system in the nuclear scale. On the other hand, the wide momentum distribution is related to the inner part of the halo neutron orbits, close to the core region.

An interesting aspect of two-neutron halo states, associated with the narrow core momentum distribution, is that the halo constituents should have a high probability to be found in the classically forbidden region, outside the potential range. Therefore, the halo wave function should be quite insensitive to details of the interactions, once the model is adjusted by the best known two- and three-body low-energy observables. Therefore, one natural observable is the two-neutron separation energy, S_{2n} , which represents the three-body binding. For the two-body subsystems neutron-neutron ($n-n$) and neutron-core ($n-c$), the appropriate observables are the corresponding scattering lengths (or, respective, two-body energies). With these arguments, studies with schematic potentials, such as contact interactions, have been quite successful in describing low-energy three-body structures for large two-body scattering lengths (when the corresponding energies are close to zero). Actually, investigations on quantum three-body systems within this regime, in nuclear and atomic physics, became quite well known in view of recent experimental realizations in atomic laboratories of the long-time predicted Efimov effect [3], which corresponds to the increasing number of excited three-body states as one goes to the unitary limit (when one or both two-body scattering lengths are close to infinity). For recent reports, quoting the main experimental realizations of this effect, see Refs. [4,5].

By considering a contact interaction, the corresponding wave-function is an eigenstate of the free Hamiltonian, except in the positions where the particles are right on the top of each other; and, therefore, the particles are in the classically forbidden region (see, e.g., [6]). Such theoretical approach applied to light-exotic nuclei close to the neutron drip-line, within a neutron-neutron-core ($n-n-c$) configuration, is described in detail in a recent review, in Ref. [7], where universal aspects of the properties of the weakly-bound $n-n-c$ systems are emphasized.

Our focus here is to present a theoretical investigation concerned to the experimental core recoil momentum distributions of the halo-nuclei ^{11}Li [1], ^{14}Be [8],

^{20}C and ^{22}C [9], as obtained by the halo breakup on nuclear targets (see also Ref. [10]). The approach is the above described three-body model, which we found appropriate for the analysis of low-binding energy systems as these ones. In the particular cases of ^{11}Li , ^{14}Be and the carbon systems ^{20}C and ^{22}C , we consider that the neutron-neutron and the neutron-core interactions are dominated by s -wave states. The calculations of core momentum distributions are performed within a renormalized zero-range three-body model, with the halo nucleus described as two neutrons with an inert core ($n-n-c$) [7,11]. The detailed expressions for the momentum distribution are given in [12], within an approach that requires as inputs one two-body ($n-c$) and one three-body ($n-n-c$) observable, given that the other two-body observable is fixed to the well-known virtual-state energy of the $n-n$ system. Usually, within such approach it is appropriate to consider the corresponding two-body scattering lengths (positive, for bound, and negative for virtual state systems); with a three-body scale given by the two-neutron separation energy, S_{2n} . Therefore, in a more general description of low-energy three-body physics with two distinguished particles ($\alpha-\alpha-\beta$), an appropriate universal scaling function is given (see e.g. [7]), where only three low-energy inputs are enough to determine any other relevant low-energy observable of the system.

Within our study on the momentum distributions of the core in halo nuclei the observable that we are concerned is the variance of the momentum distribution, given by σ^2 (associated with the normal one), which is universally correlated to the two possible scattering lengths and S_{2n} . One obtains σ from the Full Width at Half Maximum (FWHM) of the momentum distribution, such that one can find that $\text{FWHM} = 2\sqrt{2\ln 2}\sigma$. Once this quantity is known experimentally, one can use the scaling function to estimate the value of S_{2n} or, eventually, to constraint some other poorly known low-energy observable, such as a subsystem energy, or scattering length. The natural units for σ in halo physics is MeV/c . As we are interested in scaling properties of observables, it is convenient to introduce the dimensionless ratio $\sigma/\sqrt{S_{2n}m_n}$, where m_n is the neutron mass. By taking m_n as the mass unit, a scaling function can be defined, with a general form given by

$$\frac{\sigma}{\sqrt{S_{2n}}} = \mathcal{S}_c \left(\pm \sqrt{\frac{E_{nn}}{S_{2n}}}, \pm \sqrt{\frac{E_{nc}}{S_{2n}}}; A \right), \quad (1)$$

where the $+$ and $-$ signs refer to the bound and virtual subsystem energies, respectively. The core mass number is $A \equiv m_c/m_n$. The corresponding energies, E_{nn} and E_{nc} , are positive defined quantities, with a_{nn} and a_{nc} being the respective two-body scattering lengths. In our specific case of the two-neutron halo nuclei the above scaling function (1) has E_{nn} fixed to the $n-n$ virtual state. In the next, our units are such that the Planck constant \hbar and the velocity of light c are set to one. All masses are taken in units of m_n .

For the momentum distribution width, the scaling function (1) is the limit cycle of the correlation function associated with σ as a function of E_{nn} , E_{nc} and S_{2n} , when the three-body ultraviolet (UV) cut-off is driven to infinite in the three-body integral equations, or equally the scattering lengths driven to zero with a fixed UV cut-off. Similar procedure is performed within a renormalized zero-range three-body model, in the subtracted integral equations, where the subtraction energy is fixed and the two-body scattering lengths are driven towards infinite. In practice, both procedures provides very close results, as shown in Ref. [13]. In the exact Efimov limit ($E_{nn} = E_{nc} = 0$), the width is a universal function of the mass number A , $\sigma/\sqrt{S_{2n}} = \mathcal{S}_c(0, 0, A)$, which is associated to a limit cycle. Already in the first cycle it approaches the results of the renormalized zero-range three-body model (see e.g. [7]), namely given by the subtracted Skorniakov and Ter-Martirosian equations for mass imbalanced systems [14].

For the analysis of the core momentum distribution, we consider data for ^{11}Li [1], ^{14}Be [8] and ^{20}C [9] as the low-energy parameters, which are the inputs of our renormalized zero-range model. This procedure allows us to verify the utility of such “bare” formula (1), which does not include distortion effects from the scattering, to analyse the actual breakup data for those systems, taken at few-hundred MeV/A.

As an application of our model, we study in more detail the two neutron halo of the Borromean nuclei ^{22}C , in an attempt to extract information of the halo properties, by using the correlation between observables expressed in Eq.(1), namely the width of the core recoil distribution as a function of S_{2n} and the energy of the s -wave virtual state of ^{21}C . From the experimental point of view the two-neutron separation energy of ^{22}C is not well constrained, with a value of 0.42 ± 0.94 MeV given by systematics [15] and from a mass measurement, it was found $S_{2n} = -0.14(46)$ MeV[16]. There is an indirect evidence that ^{22}C could be bound by less than 70 keV [17]. Other independent information on the binding energy of this nucleus can be obtained from the matter radius. Tanaka and collaborators [18] extracted a root-mean-square (rms) matter radius of 5.4 ± 0.9 fm from the analysis of the large reaction cross sections of ^{22}C on liquid hydrogen target at 40A MeV, using a finite-range Glauber calculation under an optical-limit approximation. Furthermore, the two-valence neutrons occupy preferentially one $s_{1/2}$ orbital in their analysis. Such rms matter radius, taken together with the corresponding one of ^{20}C (2.98(5) fm[19]), suggest a halo neutron orbit with rms radius of 15 ± 4 fm in ^{22}C , which is constraining the S_{2n} to be below 100 keV [20]. This value is consistent with results obtained from a shell-model approach [21] and results from effective field theory with contact interaction [22,23]. The estimated ^{22}C quantities should be compared with the fairly small value of $S_{2n} = 369.15(65)$ keV for ^{11}Li in the nuclear scale [24], and with the neutron-neutron ($n-n$) average separation distances R_{nn} in ^{11}Li around 6-8 fm, which is obtained

from the $n - n$ correlation function measured by the breakup cross-section on heavy nuclei [25,26]. However, Riisager [2] pointed out that a comparison of experimental data obtained for the core recoil momentum distributions of ^{11}Li [1] and ^{22}C [9] suggests similar neutron halo sizes for these nuclei, which could indicate an overestimation of the matter radius of this carbon isotope.

Our present work can give more insights in resolving the issue of the size of the two neutron halo in ^{22}C . The constraints in the parameters associated with the ^{22}C halo structure and two-neutron separation energy provided by the scaling formula for the width of the core recoil momentum distribution are discussed on the basis that corresponding data, fitted to three-body model calculations. The particular case of ^{22}C is interesting considering that the corresponding observables are probably dominated by the tail of the three-body wave function in an ideal s -wave three-body model. That ideal structure was already considered in Ref. [27], within a Borromean $n - n - ^{20}\text{C}$ configuration for ^{22}C , where all two-body subsystems, $n - ^{20}\text{C}$ and $n - n$ are not bound.

As it will be shown in the following, the recent experimental results for ^{20}C and ^{22}C [9] allow us, in principle, to constraint S_{2n} and the matter radius of ^{22}C , even considering that the scattering length of the subsystem neutron- ^{20}C is not well known. From the experimental analysis performed in Ref. [17], the associated s -wave virtual-state energy of ^{21}C is found to be about 1 MeV.

The present study on the constraint for S_{2n} are relying on the applicability of the renormalized three-body zero-range model and scaling function (1) derived for the width of the core recoil momentum distribution. In the case of ^{22}C , this is obtained by fitting this distribution to the experimental breakup cross-section data given in Ref. [9]. For our estimative of S_{2n} is also essential that the scaling function given in (1) has a weak dependence of the E_{nc}/S_{2n} ratio.

One of the sources of information on the sizes of unstable neutron-rich nuclei, is the $n - n$ correlation function obtained from Coulomb breakup experiments with neutron rich projectile on heavy nuclei [28,25,26]. The experimental results for the $n - n$ correlation function for Borromean nuclei ^{11}Li and ^{14}Be are found quite consistent with the corresponding computed quantities obtained within a subtracted renormalized zero-range model [29], unless an unexpected theoretical minimum before the correlation function approach unity for large relative momentum. Data from the experiments are showing a monodic decrease of the correlation function with momentum; however, the accessible data goes only up to the predicted minima region.

Next, we present the basic formalism. In section 3 we have the main results, followed by the section 4 where we summarize our conclusions.

2 Model formalism

In the following, we briefly sketch the formalism, based on the renormalized zero-range three-body model, leading to the core recoil momentum distribution formula, which is used in our data analysis of the halo nuclei systems ^{11}Li , ^{14}Be , ^{20}C and ^{22}C .

The renormalized zero-range model which we are considering to describe the halo wave-function has been explained in detail in the review [7]. In order to build the s -wave three-body wave function for the $n-n-c$ system, one needs to solve a coupled integral equation for the independent spectator functions $\chi_{nn}(q)$ and $\chi_{nc}(q)$. Within the zero range model, a regularization is needed, which can be implemented with a cutoff momentum parameter, such as in Ref. [30], or by considering the subtraction procedure used in [31], which we follow in the present approach. Therefore, the present subtractive regularization approach for the spectator functions is performed at a given energy scale μ^2 , by the following coupled equations:

$$\begin{aligned}\chi_{nc}(q) &= \tau_{nc}(q; S_{2n}) \int_0^\infty k^2 dk \{ [\mathcal{G}_1(q, k; S_{2n}) - \mathcal{G}_1(q, k; \mu^2)] \chi_{nc}(k) + \\ &\quad + [\mathcal{G}_2(q, k; S_{2n}) - \mathcal{G}_2(q, k; \mu^2)] \chi_{nn}(k) \}, \\ \chi_{nn}(q) &= 2\tau_{nn}(q; S_{2n}) \int_0^\infty k^2 dk [\mathcal{G}_2(k, q; S_{2n}) - \mathcal{G}_2(k, q; \mu^2)] \chi_{nc}(k),\end{aligned}\tag{2}$$

where

$$\begin{aligned}\tau_{nc}(q; S_{2n}) &\equiv \sqrt{\left(\frac{A+1}{2A}\right)^3} \frac{1}{\pi} \left(\sqrt{S_{2n} + \frac{A+2}{2A+2} q^2} \mp \sqrt{E_{nc}} \right)^{-1}, \\ \tau_{nn}(q; S_{2n}) &\equiv \frac{1}{\pi} \left(\sqrt{S_{2n} + \frac{A+2}{4A} q^2} \mp \sqrt{E_{nn}} \right)^{-1},\end{aligned}\tag{3}$$

$$\begin{aligned}\mathcal{G}_1(q, k; S_{2n}) &\equiv \int_{-1}^1 dy \frac{2A}{2AS_{2n} + (A+1)(q^2 + k^2) + 2kqy}, \\ \mathcal{G}_2(q, k; S_{2n}) &\equiv \int_{-1}^1 dy \frac{2A}{2AS_{2n} + 2Aq^2 + (A+1)k^2 + 2Akqy}.\end{aligned}\tag{4}$$

The above set of coupled equations can also be derived from a renormalized Hamiltonian as shown in [7], where the associated renormalization group properties are also discussed. The minus ($-$) sign refers to a bound state subsystem and the plus sign ($+$) to a virtual state subsystem. Therefore, within the perspective of a more general $\alpha - \alpha - \beta$ system, the following cases can be described by the above coupled integral equations: *all-bound* configuration, when there is no unbound subsystems; *Borromean* configuration, when all the

subsystems are unbound; *tango* configuration [32,33,35], when we have two unbound and one bound subsystems; and *samba* configuration [31], when just one of the two-body subsystems is unbound. In the present case, as we are concerned with $n-n-c$ halo nuclei system, only *samba* and *Borromean* configurations are possible, once we take that $n-n$ is unbound with a virtual-state energy of about 143 keV. This implies that only the sign $+$ is to be considered for τ_{nn} in Eq. (3).

One can further simplify Eq. (2), for numerical purpose, by having an uncoupled integral equation for χ_{nc} :

$$\begin{aligned}\chi_{nc}(q) &= \tau_{nc}(q; S_{2n}) \int_0^\infty k^2 dk \mathcal{K}_\mu(q, k; S_{2n}) \chi_{nc}(k), \\ \mathcal{K}_\mu(q, k; S_{2n}) &\equiv [\mathcal{G}_1(q, k; S_{2n}) - \mathcal{G}_1(q, k; \mu^2)] + 2 \int_0^\infty p^2 dp \tau_{nn}(p; S_{2n}) \times \\ &\quad \times [\mathcal{G}_2(q, p; S_{2n}) - \mathcal{G}_2(q, p; \mu^2)] [\mathcal{G}_2(k, p; S_{2n}) - \mathcal{G}_2(k, p; \mu^2)].\end{aligned}\quad (5)$$

The corresponding s -wave three-body wave-function can be written in terms of the spectator functions $\chi_{nn}(q)$ and $\chi_{nc}(q)$ as:

$$\langle \vec{q}_c \vec{p}_c | \Psi \rangle = \frac{\chi_{nn}(q_c) + \chi_{nc}(|\vec{p}_c - \frac{\vec{q}_c}{2}|) + \chi_{nc}(|\vec{p}_c + \frac{\vec{q}_c}{2}|)}{S_{2n} + p_c^2 + \frac{A+2}{4A} q_c^2}, \quad (6)$$

where $\{|\vec{q}_c \vec{p}_c\rangle\}$ is the relative Jacobi momentum basis, with \vec{q}_c the relative momentum of the core to the center-of-mass of the $n-n$ system, and \vec{p}_c the relative momentum between the two neutrons. Note that, as we are going to present results corresponding to the limit cycle, namely, when all involved energies tends to zero with respect to the subtraction or regularization scale, we have dropped the regularization term in the denominator of the wave-function, which was introduced in Ref. [31]. The configuration space halo wave-function, which is given by the Fourier Transform of the momentum wave-function, is an eigenstate of the free Hamiltonian, except when two particles are at the same point, such that in our model the two halo-neutrons are always found in the classically forbidden region. This model can represent a real halo state as long as the neutrons have a large probability to be found outside of the potential range and of the core.

From the wave-function, given in momentum space by Eq. (6), we can define the core momentum distribution for the $n-n-c$ system as

$$n(q_c) = \int d^3 p_c |\langle \vec{q}_c \vec{p}_c | \Psi \rangle|^2, \quad (7)$$

with normalization such that $\int d^3 q_c n(q_c) = 1$. In the context of cold atoms the large momentum behaviour of the above momentum density has been

studied in detail for three-bosons in [34] and for mass imbalanced systems in [12]. The log-periodic solution of the spectator equations (2) in the ultraviolet limit, when $\mu \rightarrow \infty$, is the key property to derive asymptotic formulas for the one-body momentum densities. Furthermore, it was verified in [12] how the solutions of (2) approaches the log-periodic form for the higher Efimov excited states. In addition, it was shown that the density properties at low momentum behaviour are universal, namely, approach the limit-cycle already for the ground state with finite μ , and depend on the three-body binding energy and scattering lengths.

3 Results and discussion

The solution for the set of integral equations (2) provides the spectator functions and ultimately the momentum probability density (7). We start by showing results for $E_{nn} = E_{nc} = 0$, in order to study the limit-cycle for the core momentum distribution in the context of the two-neutron halo nuclei. To illustrate this limit we show in Fig. 1 the corresponding scaling function (1) for σ , in terms of the dimensionless ratio $\sigma/\sqrt{S_{2n}}$ as a function of the core mass number. Results for the ground and two excited states in Fig. 1 show that the limit-cycle is universal and in practice found for the ground state. We compare with the experimental values of $\sigma/\sqrt{S_{2n}}$ obtained for ^{11}Li , $\sigma = 21(3)\text{MeV}/c$, coming from the halo breakup reaction $^{11}\text{Li} + \text{C} \rightarrow ^9\text{Li} + \text{X}$ at 800 MeV/A [1], and for ^{14}Be , which has a FWHM = $92.7 \pm 2.7\text{MeV}/c$ for the core recoil momentum distribution [8] and $S_{2n} = 1.337\text{ MeV}$ [15]. The flattening of the scaling function for large A reaching an asymptotic value can be understood by inspecting the set of coupled equations (2) and the wave-function (6) by noticing that the limit $A \rightarrow \infty$ can be performed, where all dependences on A are cancelled out. One has to remind that even for $A \rightarrow \infty$ the dependence of the core momentum distribution on the relative momentum q_c just reflects the momentum distribution of the center of mass the two halo-neutrons in the nucleus. On the other hand, for $A \rightarrow 0$, the momentum distribution tends to be concentrated at small momentum as one can easily check that the relevant contribution to the integral equation for the spectator function comes from small momentum and $\sigma \rightarrow 0$. Naively, the light particle explores large distances, as the characteristic momentum is of the order of $\sqrt{S_{2n}/A}$, and therefore $\sigma \sim \sqrt{A}$ for $A \rightarrow 0$.

The dependence of σ on the subsystems energies E_{nn} and E_{nc} is investigated by considering the results presented in Figs. 2 and 3, where we consider the Borromean configurations, in the cases of ^{11}Li , ^{14}Be and ^{22}C , as well as the *samba* type configuration (bound *nc* subsystem), which is exemplified by the case of ^{20}C . For $E_{nc} = 0$ and by changing E_{nn} from 0 to 143 keV, σ increases

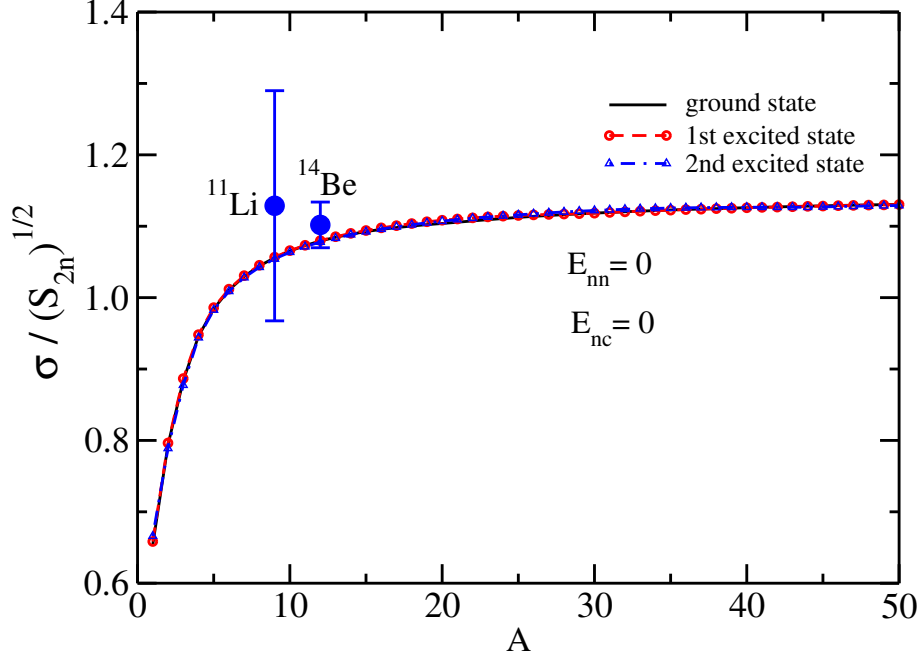


Fig. 1. Scaling plot for the core recoil momentum distribution σ in the Efimov limit as a function of the core mass number A . Experimental widths are from Refs. [1] and [8], for ^{11}Li and ^{14}Be , respectively.

with respect to $\sqrt{S_{2n}}$, as is seen when the values at the origin of these figures are compared to Fig. 1. It means that the halo shrinks as the virtual state energy increases in absolute value. This effect was found in [31], namely for a given S_{2n} the size of the halo shrinks when going from *all-bound* configuration to the *Borromean* one. This behaviour happens because the interaction becomes less attractive, such that to keep the three-body binding energy the state has to become smaller. This effect is also observed as the value of E_{nc} increases in for ^{11}Li (*left-frame*) and ^{14}Be (*right-frame*), as shown in Fig. 2. For the s -wave virtual state energy of ^{10}Li of 50 keV, one has $\sigma/\sqrt{S_{2n}} = 1.18$ and $\sigma = 22 \text{ MeV}/c$ compared to the experimental value of $\sigma = 21(3) \text{ MeV}/c$ [1]. The experimental value of $\sigma = 39.4 \pm 1.1 \text{ MeV}/c$ from the FWHM of the momentum distribution of ^{14}Be [8] is represented by the region delimited with the dashed lines in the right-frame of Fig. 2, and from that we could say roughly that s -wave virtual state of ^{13}Be E_{nc} is less than 1 MeV, which is consistent with 0.2 MeV that is the known value (see e.g. [31]). We note that the dependence on E_{nc} is very mild and by changing it from 0 to S_{2n} a variation of $\sigma/\sqrt{S_{2n}}$ of only 10% is found in our model, which puts a constraint in the error in the experimental ratio $\sigma/\sqrt{S_{2n}}$ in order to be useful to extract information on the neutron-core virtual state energy.

In Fig. 3, we show results for the scaling plots for the core momentum distribution σ in ^{20}C (*left-frame*) and ^{22}C (*right-frame*). In the left frame, the subsystem n - ^{18}C forming the s -wave one neutron halo ^{19}C is bound with energy $E_{nc} \equiv S_{1n} = 580 \text{ keV}$ [15], where S_{1n} is the one neutron separation en-

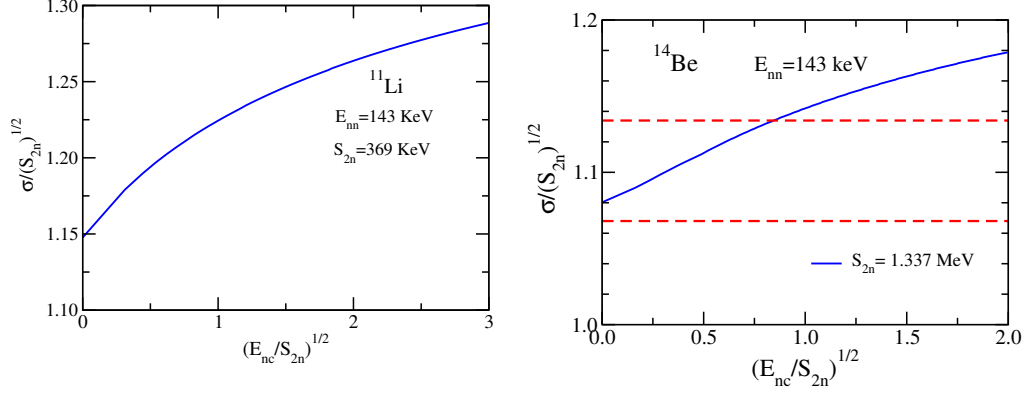


Fig. 2. Scaling plots for the core momentum distribution σ in ^{11}Li (*left-frame*) and ^{14}Be (*right-frame*) for the fixed $E_{nn} = 143\text{ keV}$ (virtual energy). The experimental $S_{2n} = 369\text{ keV}$ [24] and 1.337 MeV [15], for ^{11}Li and ^{14}Be , respectively. The dashed lines for ^{14}Be represent the region delimited by the experimental value $\text{FWHM} = 92.7 \pm 2.7\text{ MeV/c}$ [8].

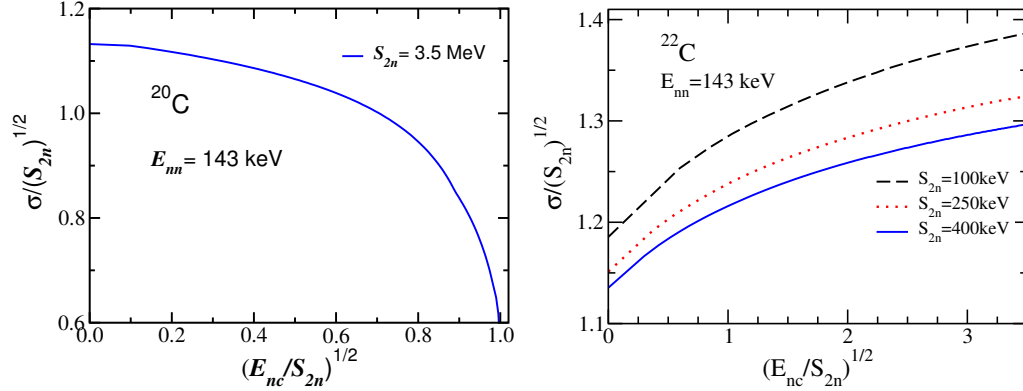


Fig. 3. Scaling plots for the core momentum distribution σ for ^{20}C (*left-frame*) and ^{22}C (*right-frame*), for a fixed $E_{nn} = 143\text{ keV}$ (virtual-state energy). In the left frame, for ^{20}C , we use $S_{2n} = 3.5\text{ MeV}$ [15]. In the right frame, for ^{22}C , we use three values for S_{2n} : 100 keV (dashed line), 250 keV (dotted line) and 400 keV (solid line).

ergy. Although, all halo low-energy scales are known for ^{20}C , we allow variation of the ratio E_{nc}/S_{2n} to illustrate how the width of the momentum distribution varies in the case of halo nuclei with bound $n - c$ subsystem. The width decreases as E_{nc}/S_{2n} increases as the bound state energy becomes closer to the lowest scattering threshold, and consequently the neutron distance to core increases leading to the sudden drop of σ to zero, when E_{nc}/S_{2n} goes to unity. In the right-frame of the figure, we present results for $\sigma/\sqrt{S_{2n}}$ as a function of $(E_{nc}/S_{2n})^{1/2}$ for ^{22}C computed with different values of S_{2n} , 100 keV , 250 keV and 400 keV . We observe in the figure that while σ exhibits a strong dependence on S_{2n} with E_{nn} and E_{nc} kept constant, the variation of σ with the ratio E_{nc}/S_{2n} for S_{2n} constant shows a quite weak sensitivity, as one could expect for the Borromean case. In that sense, as already recognized, the value of σ gives a good constraint for S_{2n} in this case.

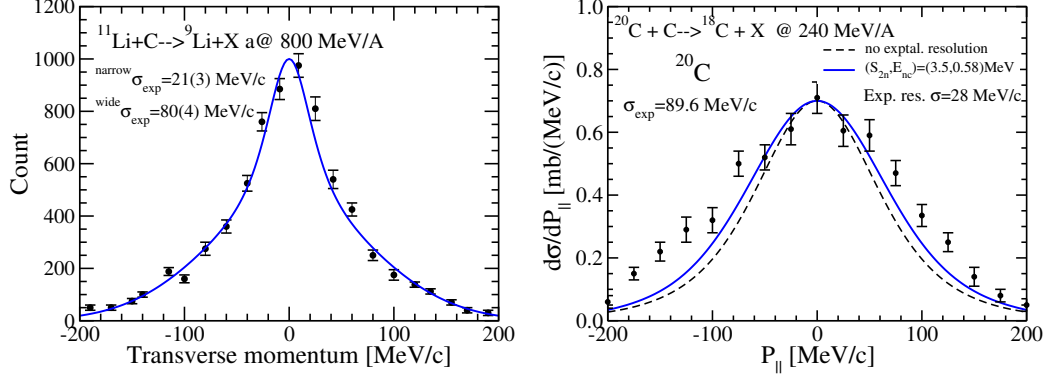


Fig. 4. Distributions of the recoil core in ^{11}Li (left-frame) and ^{20}C (right-frame) observed in the halo breakup reaction in a target compared to our calculations of the momentum distribution normalized to the data. The narrow distribution for ^{11}Li is computed with $S_{2n} = 369$ keV [24], s -wave virtual state energy of ^{10}Li , $E_{nc}=50$ keV, and singlet $n - n$ virtual state, $E_{nn}=143$ keV. The results for the distribution with the computed narrow $\sigma = 22$ MeV/c ($\sigma_{exp} = 21(3)$ MeV/c) are added to a wide one with $\sigma_{exp} = 80$ MeV/c. The calculations were performed for the experimental values from [15] of $S_{2n} = 3.5$ MeV for ^{20}C , $S_{1n} = 580$ keV for ^{19}C . The experimental results for ^{11}Li are extracted from [1] and for ^{20}C from [9]. For ^{11}Li the experiment detected the ^9Li transverse momentum to the beam and for ^{20}C the inclusive parallel momentum of ^{18}C . The distribution for ^{20}C was folded with the experimental resolution of $\sigma = 28$ MeV/c.

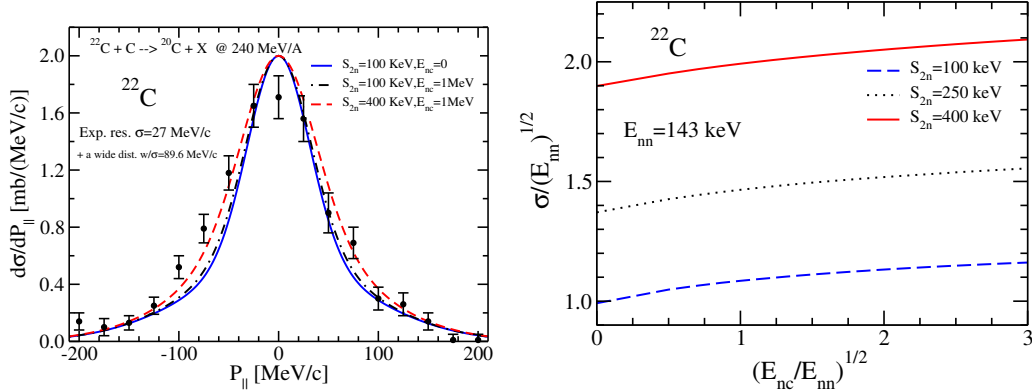


Fig. 5. *Left-frame*: Distribution of the recoil core ^{22}C obtained with the zero-range model compared to the experimental data from [9] for different inputs. For ^{22}C the experiment detected the inclusive parallel momentum of ^{20}C . Results for $(S_{2n}[\text{keV}], E_{nc}[\text{MeV}])$ folded with the experimental resolution of $\sigma = 27$ MeV/c and added to a wide distribution with $\sigma = 89.6$ MeV/c: solid-line (100,0), dashed-line (400,1) and dotted-line (100,1). *Right-frame*: Scaling plot for the core momentum width (σ) in ^{22}C (right frame) for given singlet $n - n$ virtual state energy (143 keV) and S_{2n} of 100 keV (dashed line), 250 keV (dotted line) and 400 keV (solid line).

After our discussion of the general scaling properties of the width of the momentum distribution, we show in Fig. 4 our calculations of the core recoil momentum distribution for ^{11}Li (left-frame) and ^{20}C (right-frame) compared

to actual results from halo breakup experiments obtained reactions with carbon target at 800 MeV/A [1] and at 240 MeV/A [9], respectively. For ^{11}Li , a wide distribution with $\sigma = 80$ MeV/c is added to the computed narrow one, which has $\sigma = 22$ MeV/c. We remark that all three inputs to compute the narrow distribution are fixed to known values of $S_{2n} = 369$ keV [24], the s -wave virtual state energy of ^{10}Li , $E_{nc} = 50$ keV, and the singlet $n-n$ virtual state, $E_{nn} = 143$ keV. The wide momentum distribution is beyond our model, which is more concerned on the halo neutrons. That contribution should be associated with inner part of the halo neutron orbits, close to the core region. In the comparison with the experimental data, the normalisations of the wide and narrow distributions are fitted to the data. After that, we find a fair reproduction of the experimental data as shown in the figure. This procedure confirms that our approach is a viable tool to extract information on the large two-neutron halo properties from the core momentum distribution.

The right-frame of Fig. 4 presents the core momentum distribution for ^{20}C . The calculations were performed with $S_{2n} = 3.5$ MeV and with ^{19}C one-neutron separation energy equal to 580 keV [15]. The model is compared to data obtained from [9], after folding with the experimental resolution of $\sigma = 28$ MeV/c. We observe that a wide distribution is somewhat missing to fit the experimental results in this case.

The model results for the core recoil momentum distribution in ^{22}C , with two-neutron separation energies of 100 and 400 KeV, is presented in the left-frame of Fig. 5, and compared to data obtained from [9]. The singlet virtual $n-n$ energy is fixed to 143 keV, with the virtual-state energy of $n-^{20}\text{C}$ chosen as 0 and 1 MeV [17]. The narrow theoretical distribution is folded to the experimental resolution of $\sigma = 27$ MeV/c and added to a wide one with $\sigma = 89.6$ MeV/c. The results presented in this figure illustrate the weak sensitivity of the core recoil momentum distribution to the variation of the virtual-state energy of ^{21}C , which is taken between 0 and 1 MeV, as it was shown by the results with $S_{2n} = 100$ keV. The difference between the distributions obtained with $S_{2n} = 100$ and 400 keV, computed with $E_{nc} = 1$ MeV is not enough to discriminate S_{2n} in view of the experimental data error. The model sensitivity to the physical inputs, in the interesting case of ^{22}C is further explored, in the right-frame of the figure, where the scaling plot for $\sigma/\sqrt{E_{nn}}$ as a function of $\sqrt{E_{nc}/E_{nn}}$ is shown for three values of S_{2n} . The weak sensitivity to the s -wave virtual state energy of ^{21}C is seen and one could consider to obtain an upper limit to the experimental relative error in order to extract information on the $n-^{20}\text{C}$ scattering length. However, a variation of the ratio E_{nc}/E_{nn} between 0 and 9 gives 10% variation of σ (E_{nn} is fixed), which is surmounted by a variation of about 50% in S_{2n} . Therefore, it is required an independent source of information to constrain the $n-^{20}\text{C}$ scattering length, which we can find from the matter radius of ^{22}C [18].

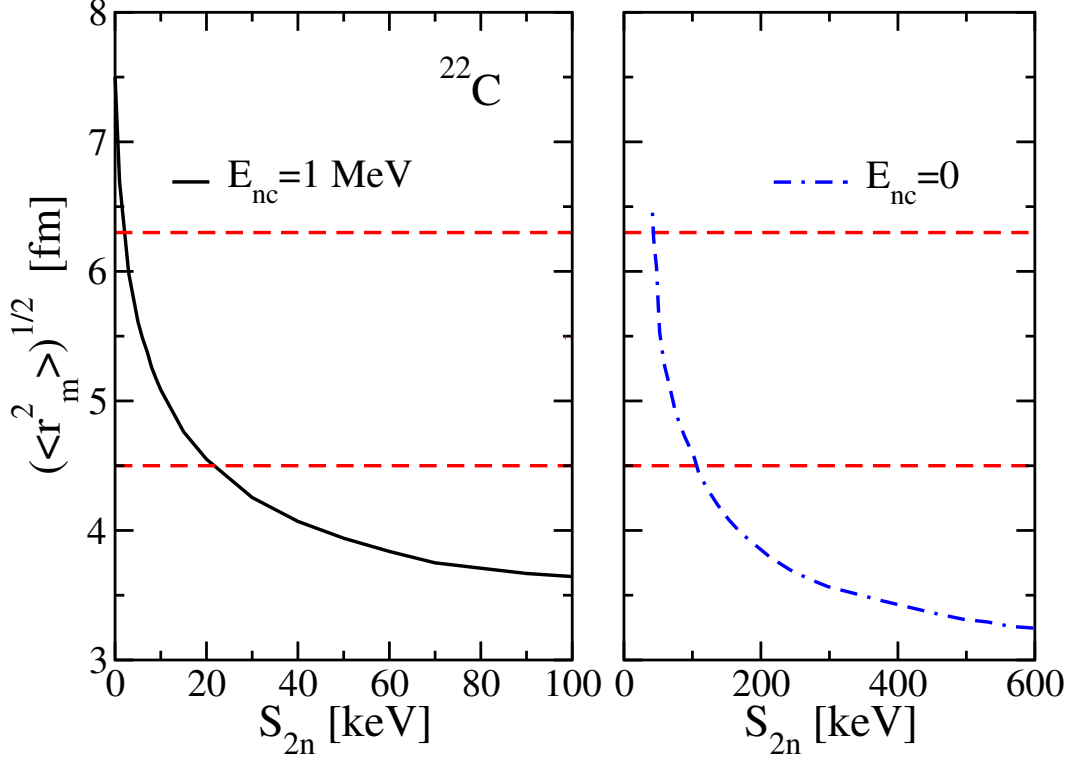


Fig. 6. Root-mean-square (rms) matter radius of ^{22}C given as a function of the two-neutron separation energy, computed with the singlet $n-n$ virtual-state energy fixed ($E_{nn} = 143$ keV), considering the virtual-state energy of $n-^{20}\text{C}$ given by $E_{nc} = 1$ MeV (left frame) and 0 MeV (right frame). The dashed lines represent the upper and lower limits for the experimental value 5.4 ± 0.9 fm reported in [18].

To close our discussion of ^{22}C , we computed the matter radius starting with the rms radius of the halo neutrons (r_n) with respect to the center-of-mass, which is obtained from the configuration space $n-n-c$ wave-function, which is obtained by considering the Fourier transform of the corresponding momentum wave-function (6). For details on this procedure, see [31,20]. The corresponding formula of the matter radius is given by $\sqrt{\langle r_m^2[^{22}\text{C}] \rangle} = \sqrt{(2/22) \langle r_n^2 \rangle + (20/22) \langle r_m^2[^{20}\text{C}] \rangle}$. The ^{20}C matter radius is $r_m[^{20}\text{C}] = 2.98(5)$ fm [19]. The plot of Fig. 6 shows the theoretical values of the rms matter radius of ^{22}C as a function of S_{2n} for a fixed s -wave virtual state energies of the singlet $n-n$ pair (143 keV) and ^{21}C (1 MeV [17] and 0) compared to data from [18]. In the figure, the limits for the extracted matter radius [18] are shown, and we can make some remarks analysing the consistence between the different available data and our model, considering that $100 \text{ keV} \lesssim S_{2n} \lesssim 400 \text{ keV}$: (i) for $E_{nc} = 0$, one finds that $3.5 \text{ fm} \lesssim \langle r_m^2[^{22}\text{C}] \rangle^{1/2} \lesssim 4.5 \text{ fm}$; and, (ii) for $E_{nc} = 1$ MeV, we have $\langle r_m^2[^{22}\text{C}] \rangle^{1/2} \lesssim 3.5 \text{ fm}$. Only if $E_{nc} \sim 0$ we obtain a region for S_{2n} close to 100 keV, consistent with rms matter radius of ^{22}C within one standard deviation and in the lower bound of the radius, namely ~ 4.5 fm. The value of $E_{nc} = 1$ MeV for the virtual state of ^{21}C and $S_{2n} \sim$

100 keV is compatible with two standard deviation; from that, $\langle r_m^2[{}^{22}\text{C}] \rangle^{1/2} \lesssim 3.5$ fm. This combined analysis for ${}^{22}\text{C}$ of the core recoil momentum distribution, with rms matter radius and virtual state energy of $n-{}^{20}\text{C}$, suggests that such virtual-state energy and matter radius are overestimated. Independent new data on the S_{2n} for ${}^{22}\text{C}$ could help in clarifying the tension between data analysis with the present universal model.

4 Conclusions

In summary, by considering the renormalized zero-range model applied to the case of core recoil momentum distributions of ${}^{11}\text{Li}$ and ${}^{14}\text{Be}$, we found a fair consistency with experimental data, just by using the known low-energy parameters. Relying on the fact that such simplified model gives already a valid description of the two-neutron s -wave halo, we proceed with a combined analysis of recent experimental data on the core momentum distribution in ${}^{22}\text{C}$, which is given by Kobaiashi et al. [9], the corresponding rms matter radius and the ${}^{21}\text{C}$ virtual state energy. Our conclusion is that, with the value of the two-neutron separation energy of ${}^{22}\text{C}$ given in the interval from 100 to 400 keV, the rms matter radius of ${}^{22}\text{C}$ will be within two standard deviations if the virtual state energy of ${}^{21}\text{C}$ is close to 0. By considering the ${}^{21}\text{C}$ with a virtual-state energy between 0 and 1 MeV, the matter rms radius should be between 3.5 and 4.5 fm. To reconcile a virtual-state energy with $E_{nc} \sim 1$ MeV, a matter radius of 5.4 ± 0.9 fm and $100 \text{ keV} \lesssim S_{2n} \lesssim 400 \text{ keV}$, the possibility is $S_{2n} \sim 100 \text{ keV}$ and $E_{nc} < 1 \text{ MeV}$, implying that $\langle r_m^2[{}^{22}\text{C}] \rangle^{1/2} \sim 4.5$ fm. A refined analysis of the core momentum distribution, beyond the Serber model [36], is desirable, of course. However, the comparison of results obtained by the present model for ${}^{11}\text{Li}$ and ${}^{14}\text{Be}$ with corresponding data suggests small corrections to the distribution verified for ${}^{22}\text{C}$.

We thank partial support from the Brazilian agencies FAPESP, CNPq and CAPES.

References

- [1] I. Tanihata, J. Phys. G **22** (1996) 157.
- [2] K. Riisager, Phys. Scr. T**152** (2013) 014001.
- [3] V. Efimov, Phys. Lett. B **33** (1970) 563.
- [4] V. Efimov, Few-Body Syst. **51** (2011) 79.
- [5] F. Ferlaino, A. Zenesini, M. Berninger, B. Huang, H.-C. Nägerl, and R. Grimm, Few-Body Syst. **51** (2011) 113.

- [6] T. Frederico, *Few-Body Syst.* **55** (2014) 651.
- [7] T. Frederico, M. T. Yamashita, A. Delfino, and L. Tomio, *Prog. Part. Nucl. Phys.* **67** (2012) 939.
- [8] M. Zahar, et al., *Phys. Rev. C* **48** (1993) R1484.
- [9] N. Kobayashi et al., *Phys. Rev. C* **86** (2012) 054604.
- [10] I. Tanihata, H. Savajols, and R. Kanungo, *Prog. Part. Nucl. Phys.* **68** (2013) 215.
- [11] T. Frederico, L. Tomio, A. Delfino, M. R. Hadizadeh, M. T. Yamashita, *Few-Body Syst.* **51** (2011) 87.
- [12] M. T. Yamashita, F. F. Bellotti, T. Frederico, D. V. Fedorov, A. S. Jensen, N. T. Zinner, *Phys. Rev. A* **87** (2013) 062702.
- [13] M. T. Yamashita, T. Frederico, A. Delfino, L. Tomio, *Phys. Rev. A* **66** (2002) 052702.
- [14] G. A. Skorniakov, K. A. Ter-Martirosian. *Sov. Phys. JETP* **4** (1957) 648.
- [15] G. Audi, A. H. Wapstra, and C. Thibault, *Nucl. Phys. A* **729**, 337 (2003).
- [16] L. Gaudefroy et al., *Phys. Rev. Lett.* **109** (2012) 202503.
- [17] S. Mosby et al., *Nucl. Phys. A* **909**, 69-78 (2013)
- [18] K. Tanaka *et al.*, *Phys. Rev. Lett.* **104** (2010) 062701.
- [19] A. Ozawa et al., *Nucl. Phys. A* **691** (2001) 599.
- [20] M. T. Yamashita, R. M. de Carvalho, T. Frederico, L. Tomio, *Phys. Lett. B* **697** (2011) 90; *Phys. Lett. B* **715** (2012) 282.
- [21] H. T. Fortune, R. Sherr, *Phys. Rev. C* **85** (2012) 027303.
- [22] B. Acharya, C. Ji, D. R. Phillips, *Phys. Lett. B* **723** (2013) 196.
- [23] B. Acharya, D. R. Phillips, arXiv:1508.02697 [nucl-th]. Contribution to the 21st Conference in Few-Body Problems in Physics.
- [24] M. Smith et al., *Phys. Rev. Lett.* **101** (2008) 202501.
- [25] F. M. Marqués, et al., *Phys. Rev. C* **64** (2001) 061301.
- [26] M. Petrascu, et al., *Nucl. Phys. A* **738** (2004) 503.
- [27] W. Horiuchi and Y. Suzuki, *Phys. Rev. C* **74** (2006) 034311.
- [28] F. M. Marqués, et al. *Phys. Lett. B* **476** (2000) 219.
- [29] M. T. Yamashita, T. Frederico, L. Tomio, *Phys. Rev. C* **72** (2005) 011601(R).
- [30] A. E. A. Amorim, T. Frederico and L. Tomio, *Phys. Rev. C* **56** (1997) R2378.

- [31] M. T. Yamashita, L. Tomio, T. Frederico, Nucl. Phys. A **735** (2004) 40.
- [32] F. Robicheaux, Phys. Rev. A **60** (1999) 1706.
- [33] A. S. Jensen, K. Riisager, D.V. Fedorov, E. Garrido, Rev. Mod. Phys. **76** (2004) 215.
- [34] Y. Castin and F. Werner, Phys. Rev. A **83** (2011) 063614.
- [35] N. T. Zinner, A. S. Jensen, J. Phys. G: Nucl. Part. Phys. **40** (2013) 053101.
- [36] R. Serber, Phys. Rev. **72** (1947) 1008.